Average shot-noise power via a diagrammatic method

2010 J. Phys. A: Math. Theor. 43 075101

(http://iopscience.iop.org/1751-8121/43/7/075101)

J. Phys. A: Math. Theor. **43** (2010) 075101 (16pp) doi:10.1088/1751-8113/43/7/075101

Average shot-noise power via a diagrammatic method

A L R Barbosa, J G G S Ramos and A M S Macêdo

Departamento de Física, Laboratório de Física Teórica e Computacional, Universidade Federal de Pernambuco 50670-901 Recife, Pernambuco, Brazil

Received 2 September 2009, in final form 28 November 2009
Published 1 February 2010
Online at stacks.iop.org/JPhysA/43/075101

Abstract
In this work we use a diagrammatic method for integration over the unitary group to obtain a quantum correction to the average shot-noise power of a chaotic cavity with non-ideal contacts. We present maximally crossed diagrams representing the physical modes of the system responsible for the dominant quantum correction. We demonstrate with explicit calculations that the suppression–amplification effect reported in Ramos *et al* (2008 *Phys. Rev.* B **78** 235305) occurs both for systems in the presence of time-reversal (TR) and spin-rotation (SR) symmetries and for systems with broken SR symmetry but in the presence of TR symmetry.

PACS numbers: 73.23.−b, 73.21.La, 05.45.Mt

1. Introduction

The study of statistical features of transport observables in quantum electron devices has always been of great theoretical and experimental interest in the community of mesoscopic physics [1–5]. The main transport observables of mesoscopic structures such as quantum dots and quantum wires are the conductance and the shot-noise power [6, 7]. Both quantities can exhibit detectable quantum interference effects which are caused by multiple coherent scattering in the system. One of the most important types of quantum interference effect is weak localization (WL), which corresponds to a suppression of the average conductance of systems in the presence of both time-reversal (TR) and spin-rotation (SR) symmetries. Present technology makes it possible to have control over many experimental parameters such as temperature, magnetic field and barriers' transparencies [8, 9] so that measurements of the WL correction are a great source of information about the underlying mechanisms of the quantum coherent dynamics in the system. The best studied type of WL correction corresponds to a suppression of the average conductance and represents an important probe on quantum mechanisms that depends on fundamental time scales [10–12], such as the Ehrenfest time τ_E, the dwell time $\tau_{\rm dw}$ and the ergodic time $\tau_{\rm erg}$.

Recent theoretical efforts have been directed to the understanding of the WL correction to the average shot-noise power of quantum dots [13–15]. Braun *et al* [13] used a semiclassical

trajectory approach to describe the orthogonal-unitary crossover, i.e. the gradual breaking of TR symmetry by an applied magnetic field. Employing random-matrix theory [16], Savin and Sommers [14] calculated analytically exact expressions for the average shot-noise power. Béri and Cserti [15] extended the results of [13] to a very general class of crossover that includes simultaneously spin–orbit coupling and an external magnetic field. We note that the above results are restricted to chaotic cavities with ideal contacts. When barriers of arbitrary transparencies are present, which is the case of non-ideal contacts, we showed in [17] that new surprising effects can emerge, such as the suppression–amplification transition of the average shot-noise power, caused by gradually changing the transparencies of the barriers. The present work is an extension of [17]. We provide a detailed account of the very subtle selection of maximally crossed diagrams that contribute to the weak-localization correction to the shot-noise power, which are essential to the final results but were only briefly discussed in [17]. We also indicate potential applications of the new set of maximally crossed diagrams in more general situations.

Random-matrix theory (RMT) describes very accurately the universal statistical properties of quantum transport observables of open chaotic cavities. The universal description is valid provided $\tau_{\rm dw} \gg \max(\tau_E, \tau_{\rm erg})$. In the case of ideal contacts it amounts to a description in terms of random scattering matrices from the standard Wigner–Dyson ensembles [3]. These ensembles are classified according to certain fundamental symmetries left unbroken by the chaotic dynamics and can be labelled by Dyson's integer index β [18]. More specifically, the circular orthogonal ensemble (COE) is applicable to systems in the presence of both TR and SR symmetries, $\beta = 1$; the circular unitary ensemble (CUE) is valid for systems in the absence of both TR and SR symmetries, $\beta = 2$; and the circular symplectic ensemble (CSE) can be used in systems with broken SR symmetry but in the presence of TR symmetry, $\beta = 4$. The basic mathematical object of the theory, the scattering matrix, can always be written in 2×2 block form as

$$S = \begin{pmatrix} r & t \\ t' & r' \end{pmatrix}, \tag{1}$$

where t, t' and r, r' are, respectively, transmission and reflection matrices. Using the Landauer scattering approach to quantum transport [1], we can relate certain moments of the transmission matrix to transport observables. For instance, the conductance is simply given by

$$\mathbf{g}_1 = \mathbf{Tr}(tt^\dagger). \tag{2}$$

Introducing the second moment

$$\mathbf{g}_2 = \mathbf{Tr}[(tt^\dagger)^2], \tag{3}$$

we can express the shot-noise power combining (2) with (3) as follows:

$$\mathbf{p} = \mathbf{g}_1 - \mathbf{g}_2 = \mathbf{Tr}[tt^\dagger(1 - tt^\dagger)]. \tag{4}$$

In order to obtain statistical properties of transport observables of a chaotic cavity with arbitrary barriers, we must use a distribution of scattering matrices that is different from the circular ensembles. Such distribution can be obtained from a *maximum information entropy principle* and is known as the Poisson kernel [19]. It reads

$$P(S) \propto |\det(1 - \bar{S}^\dagger S)|^{-(\beta N + 2 - \beta)}, \tag{5}$$

where $\beta \in \{1, 2, 4\}$ is the parameter identifying the distinct symmetry classes. The integer parameter N is the number of open scattering channels in the metallic leads that connect the

chaotic cavity to electron reservoirs and $\bar{S}$ is a sub-unitary matrix representing the average S-matrix and can without loss of generality be written as

$$\bar{S} = \begin{pmatrix} r_1 & 0 \\ 0 & r_2 \end{pmatrix}, \tag{6}$$

where r_1 and r_2 are reflection matrices of barriers 1 and 2, respectively. Note, in particular, that if we set $\bar{S} = 0$, we recover the Wigner–Dyson ensembles, since they represent uniform distributions.

The diagrammatic method used in this work was designed in [20] as a method for integration over the unitary group. It applies straightforwardly to circular ensembles and with simple modifications it can also be used for calculating averages over the Poisson kernel. It also gives a simple diagrammatic representation of the diffuson (ladder diagrams) and cooperon (maximally crossed diagrams) modes of localization theory [4, 21] in the form that it applies to open quantum dots. We believe the results of this work to be particularly relevant to further development of the diagrammatic method as a powerful tool in mesoscopic physics. The paper is organized as follows. In section 2, we provide a simple application of the diagrammatic method by deriving the exact average shot-noise power of a chaotic cavity with ideals contacts. In section 3, we present in detail the perturbative diagrammatic calculation of the average shot-noise power of a chaotic cavity with barriers giving special attention to the dominant quantum correction. A summary and conclusions are presented in section 4.

2. Average shot-noise power of a chaotic cavity with ideal contacts

In this section, we derive an exact expression for the average shot-noise power of a chaotic cavity with two ideal contacts via the diagrammatic method. From (4) we see that the average shot-noise power can be obtained by subtracting the average second moment, equation (3), from the average conductance, equation (2). The average conductance was obtained from the diagrammatic technique by Brouwer and Beenakker [20]. It reads

$$\langle \mathbf{g}_1 \rangle = \frac{N_1 N_2}{N - 1 + \frac{2}{\beta}}, \tag{7}$$

where $\beta \in \{1, 2, 4\}$ is Dyson's symmetry index, N_1 and N_2 are the numbers of open scattering channels in leads 1 and 2, respectively, so that $N = N_1 + N_2$ is the total number of open scattering channels in the system.

Thus, it remains to calculate the average second moment. Following [20] we rewrite the second moment as follows:

$$\mathbf{g}_2 = \mathbf{Tr}[(C_1 S C_2 S^\dagger)^2]. \tag{8}$$

The S-matrix in this formula can be represented as in (1) and describes the chaotic scattering inside the dot. It is distributed according to the relevant circular ensemble: COE for $\beta = 1$, CUE for $\beta = 2$ and CSE for $\beta = 4$. The matrices $C_{1,2}$ are projection matrices defined by

$$C_1 = \begin{pmatrix} 1_{N_1} & 0 \\ 0 & 0 \end{pmatrix}, \qquad C_2 = \begin{pmatrix} 0 & 0 \\ 0 & 1_{N_2} \end{pmatrix}, \tag{9}$$

where 1_{N_j} is the $N_j \times N_j$ unity matrix. The following relation hold $C_1 C_2 = 0$ and $C_1 + C_2 = 1_N$.

We are now in a position to apply the diagrammatic method for calculating the average of (8). The diagrammatic rules consist in accounting for all possible contractions of indices of scattering matrices. Black and white dots represent that the indices and contractions are

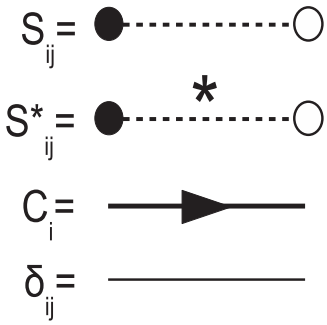

Figure 1. Basic objects of the diagrammatic rules. In decreasing order, a random element of the scattering matrix and its complex conjugate, a projector in channel space and a Kronecker delta element for contraction of indices.

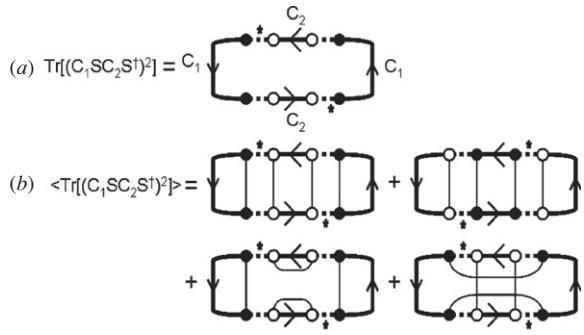

Figure 2. Diagrammatic representation of (*a*) the second moment, equation (8), and (*b*) the ensemble average of the second moment, equation (10). Note that in the language of cycles introduced in [20], the first two diagrams of (*b*) have two *U*-cycles and three *T*-cycles while the last two of them have one *U*-cycle and four and two *T*-cycles, respectively.

indicated as lines connecting the dots. A summary of the basic rules is given below.

- Draw the basic elements according to figure 1.
- Connect each possible pairing of black dots of S and S^* matrices and do the same for the white dots.
- Denote a U-cycle any closed circuit in the diagram with an alternating sequence of thick dotted lines and thin lines. U cycles have weight given by V_P, where P characterizes the permutation of indices.
- Denote a T-cycle any closed circuit with an alternating sequence of directed thick solid line and thin lines. T cycles correspond to the trace of the matrices in the circuit.

For a full description of the diagrammatic method for averaging over the Dyson ensembles CUE, COE and CSE, see [20]. Here we shall consider in detail only the CUE case, although the final expressions are extended to the other ensembles via the insertion of Dyson's index β.

The first step is to represent $\mathbf{g}_2$ diagrammatically as shown in figure 2(*a*), in which the scattering matrix is represented by thick dotted lines, $\bullet \cdots \circ$, and the projection matrices $C_{1,2}$ are represented by directed thick solid lines, see figure 1. The second step is to perform the ensemble average directly on the diagrammatic representation by connecting, in the case of

CUE, the dots of the same colour by thin lines in all topologically distinct ways. We find four possible diagrams, see figure 2(*b*). Similar diagrams have been presented in the perturbative calculation of [15]. Applying the diagrammatic rules to the diagrams of figure 2(*b*), we obtain

$$\begin{aligned}\langle \mathbf{g}_2 \rangle = {} & V_{1,1}[(\mathbf{Tr}\, C_1)^2\, \mathbf{Tr}(C_2)^2 + \mathbf{Tr}(C_1)^2 (\mathbf{Tr}\, C_2)^2] \\ & + V_2[(\mathbf{Tr}\, C_1)^2 (\mathbf{Tr}\, C_2)^2 + \mathbf{Tr}(C_1)^2\, \mathbf{Tr}(C_2)^2], \end{aligned} \tag{10}$$

where the weights are given by $V_{1,1} = (N^2-1)^{-1}$ and $V_2 = -(N(N^2-1))^{-1}$. For more details on how to calculate these weights recursively, see [20, 22]. After some algebra we obtain from (10) the following simple exact expression:

$$\langle \mathbf{g}_2 \rangle = \frac{N_1 N_2 \left(N_1^2 + N_1 N_2 + N_2^2 - 1\right)}{(N-1)N(N+1)}. \tag{11}$$

At this point we may introduce the index β and rewrite this expression in a way that is valid for all symmetry classes, as can be obtained by applying the diagrammatic rules for ensemble averaging over the COE and CSE ensembles. We find

$$\langle \mathbf{g}_2 \rangle = \frac{N_1 N_2 \left(N_1^2 + N_1 N_2 + N_2^2 - 2N + 1 + \frac{4N-6}{\beta} + \frac{4}{\beta^2}\right)}{\left(N - 2 + \frac{2}{\beta}\right)\left(N - 1 + \frac{2}{\beta}\right)\left(N - 1 + \frac{4}{\beta}\right)}. \tag{12}$$

Note that if we set $\beta = 2$ we recover (11), as expected.

Inserting (12) and (7) into $\langle \mathbf{p} \rangle = \langle \mathbf{g}_1 \rangle - \langle \mathbf{g}_2 \rangle$, we obtain the following exact expression for the average shot-noise power:

$$\langle \mathbf{p} \rangle = \frac{N_1 N_2 \left(N_1 - 1 + \frac{2}{\beta}\right)\left(N_2 - 1 + \frac{2}{\beta}\right)}{\left(N - 2 + \frac{2}{\beta}\right)\left(N - 1 + \frac{2}{\beta}\right)\left(N - 1 + \frac{4}{\beta}\right)}, \tag{13}$$

in complete agreement with [14], for arbitrary N_1 and N_2, and with [23], for $N_1 = N_2$, where the calculations were performed with non-diagrammatic methods. It is instructive to obtain from (12) and (13) the first two terms in the perturbative semiclassical expansion, which is valid provided $N_1, N_2 \gg 1$. We obtain the following expression for the average second moment:

$$\langle \mathbf{g}_2 \rangle = \frac{N_1 N_2 \left(N_1^2 + N_1 N_2 + N_2^2\right)}{(N_1 + N_2)^3} + 2\left(1 - \frac{2}{\beta}\right) \frac{N_1 N_2 \left(N_1^2 + N_2^2\right)}{(N_1 + N_2)^4} + \mathcal{O}(N^{-1}), \tag{14}$$

and for the average shot-noise power we get

$$\langle \mathbf{p} \rangle = \frac{N_1^2 N_2^2}{(N_1 + N_2)^3} - \left(1 - \frac{2}{\beta}\right) \frac{N_1 N_2 \left(N_1 - N_2\right)^2}{(N_1 + N_2)^4} + \mathcal{O}(N^{-1}). \tag{15}$$

Equation (15) is well known in the literature, see e.g. [2]. The second term in the expansion is the dominant quantum correction to the semiclassical limit. Note that if we set $\beta = 2$ in (15) the quantum correction vanishes, as expected from the suppression quantum interference caused by breaking the TR symmetry through the application of an external magnetic field. However, for $\beta = 1$ ($\beta = 4$), the quantum interference correction amplifies (suppresses) the dominant semiclassical value of the average shot-noise power and it vanishes if $N_1 = N_2$.

The calculation of the average shot-noise power of a chaotic cavity with two ideal contacts is a very simple application of the diagrammatic technique which yields exact results. In spite of the simplicity, the four diagrams of figure 2(*b*) are still a useful guide in setting up the much more complicated calculation of the perturbative expansion of the average shot-noise power of a chaotic cavity with two barriers, which is the subject of the next section.

3. Average shot-noise power of a chaotic cavity with barriers

In this section, we set up a perturbative diagrammatic procedure to calculate the average shot-noise power of a chaotic cavity with two barriers of arbitrary transparencies, with special attention to the leading quantum interference correction. In the presence of barriers, the scattering matrix of the chaotic cavity is distributed according to the Poisson kernel, equation (5). The central idea of the scheme is to map the ensemble average over the Poisson kernel onto an effective problem with a random matrix belonging to one of the circular ensembles, so that the diagrammatic technique used in the previous section applies. Following [20] this is achieved by separating the average and the fluctuating part of the scattering matrix as follows, $S = \bar{S} + \delta S$, where $\bar{S}$ is the sub-unitary matrix shown in (6). The fluctuating part is parametrized in the following form: $\delta S = L(1 - UR)^{-1}UT$, where the matrix U is a random matrix distributed according to one of the circular ensembles. The matrices L, T and R describe transmission and reflection coefficients of the barriers and are related to $\bar{S}$ via the condition that

$$\hat{\Sigma} = \begin{pmatrix} \bar{S} & L \\ T & R \end{pmatrix} \tag{16}$$

be unitary. The most convenient choices for the matrices T, L and R are

$$T = \begin{pmatrix} (\mathrm{i}\sqrt{\Gamma_1})1_{N_1} & 0 \\ 0 & (\mathrm{i}\sqrt{\Gamma_2})1_{N_2} \end{pmatrix} = L \tag{17}$$

and

$$R = \begin{pmatrix} (\sqrt{1-\Gamma_1})1_{N_1} & 0 \\ 0 & (\sqrt{1-\Gamma_2})1_{N_2} \end{pmatrix} = \bar{S}, \tag{18}$$

where Γ_1 and Γ_2 represent the transmission coefficients of each channel in barriers 1 and 2, respectively. Using the decomposition $S = \bar{S} + \delta S$ and simple statistical properties of δS, such as its vanishing average, we may write (8) as

$$\langle \mathbf{g}_2 \rangle = \langle \mathbf{Tr}[(C_1 \delta S C_2 \delta S^\dagger)^2] \rangle. \tag{19}$$

Expanding the denominator in the parametrization of δS and inserting the result in (19) we obtain the series

$$\langle \mathbf{g}_2 \rangle = \sum_{k,l,m,n \geqslant 1}^{\infty} \langle f_{k,l,m,n} \rangle, \tag{20}$$

where

$$f_{k,l,m,n} = \mathbf{Tr}[C_1 L (UR)^{k-1} U T C_2 T^\dagger U^\dagger (R^\dagger U^\dagger)^{l-1} L^\dagger C_1 L (UR)^{m-1} U T C_2 T^\dagger U^\dagger (R^\dagger U^\dagger)^{n-1} L^\dagger]. \tag{21}$$

It follows from a simple property of averages over the unitary group that $\langle f_{k,l,m,n} \rangle \neq 0$ if and only if $k + m = l + n$. The remaining non-trivial task is to calculate perturbatively the non-vanishing part of $\langle f_{k,l,m,n} \rangle$. The leading term, which yields the dominant semiclassical value, is calculated in the next section.

3.1. Dominant semiclassical term

Since the dominant semiclassical term is independent of the symmetry index β, we may perform the ensemble average using the simpler diagrammatic rules of the CUE ensemble.

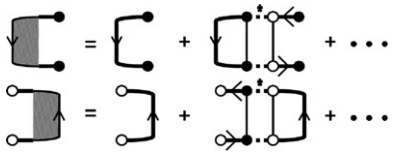

Figure 3. Diagrammatic representation of the matrices F_L (top), equation (22), and F_R (bottom), equation (23). They are an infinite series of ladder diagrams, see [20].

Table 1. Algebraic expressions corresponding to the diagrams of figure 4.

1	$W_2(\mathbf{Tr}\,F_L)^2(\mathbf{Tr}\,F_R)^2$
2	$W_1^4(\mathbf{Tr}\,F_L)^2(\mathbf{Tr}\,RR^\dagger RR^\dagger)(\mathbf{Tr}\,F_R)^2$
3	$2W_1^3(\mathbf{Tr}\,F_L)^2(\mathbf{Tr}\,TC_2T^\dagger RR^\dagger)(\mathbf{Tr}\,F_R)$
4	$2W_1^3(\mathbf{Tr}\,F_L)\left(\mathbf{Tr}L^\dagger C_1 LR^\dagger R\right)(\mathbf{Tr}\,F_R)^2$
5	$W_1^2\,\mathbf{Tr}(L^\dagger C_1 L)^2(\mathbf{Tr}\,F_R)^2$
6	$W_1^2(\mathbf{Tr}\,F_L)^2\,\mathbf{Tr}(TC_2T^\dagger)^2$

It follows that the leading contribution is given by the insertion of ladder diagrams in the first three diagrams of figure 2(*b*). In order to systematize the procedure it is convenient to introduce left and right insertions of ladder diagrams through the matrices F_L and F_R defined by

$$F_L = L^\dagger C_1 L + \sum_{n=1}^{\infty} W_1^n \mathbf{Tr}(L^\dagger C_1 L)(\mathbf{Tr}(R^\dagger R))^{n-1} R^\dagger R = L^\dagger C_1 L + \frac{\mathbf{Tr}(L^\dagger C_1 L)}{N - \mathbf{Tr}(R^\dagger R)} R^\dagger R \tag{22}$$

and

$$F_R = TC_2T^\dagger + \sum_{n=1}^{\infty} W_1^n RR^\dagger(\mathbf{Tr}(R^\dagger R))^{n-1}\,\mathbf{Tr}(TC_2T^\dagger) = TC_2T^\dagger + RR^\dagger \frac{\mathbf{Tr}(TC_2T^\dagger)}{N - \mathbf{Tr}(R^\dagger R)}, \tag{23}$$

in which we used the asymptotic value of the weight $V_1 = W_1 \approx N^{-1}$ associated with short U-cycles. These matrices are represented diagrammatically in figure 3.

We identified six topologically distinct diagrams that are shown in figure 4. For convenience we drew each diagram of figure 4 with four arms irrespective of whether there is or not an insertion of ladder diagrams. The first diagram of figure 2(*b*) generates diagrams 2, 3 and 5 of figure 4, while the second diagram generates diagrams 4 and 6. The third diagram of figure 2(*b*) generates diagram 1 of figure 4 and the last one does not generate any contribution in the semiclassical limit. These six diagrams exhibit insertions of ladder diagrams and represent the information contained in the discrete diffuson modes of the system [4].

In table 1 we show the algebraic expressions with the corresponding weights associated with each of the diagrams of figure 4. Note that the diagram of figure 4(1) has a long U-cycle with weight $V_2 = W_2$ while the others have short U-cycles with weight W_1. Adding the equations of table 1, we get

$$\begin{aligned}\langle \mathbf{g}_2 \rangle = {} & W_2(\mathbf{Tr}\,F_L)^2(\mathbf{Tr}\,F_R)^2 + W_1^4(\mathbf{Tr}\,F_L)^2(\mathbf{Tr}\,RR^\dagger RR^\dagger)(\mathbf{Tr}\,F_R)^2 \\ & + 2W_1^3(\mathbf{Tr}\,F_L)^2(\mathbf{Tr}\,TC_2T^\dagger RR^\dagger)(\mathbf{Tr}\,F_R) + 2W_1^3(\mathbf{Tr}\,F_L)(\mathbf{Tr}L^\dagger C_1 LR^\dagger R)(\mathbf{Tr}\,F_R)^2 \\ & + W_1^2\,\mathbf{Tr}(L^\dagger C_1 L)^2(\mathbf{Tr}\,F_R)^2 + W_1^2(\mathbf{Tr}\,F_L)^2\,\mathbf{Tr}(TC_2T^\dagger)^2. \end{aligned} \tag{24}$$

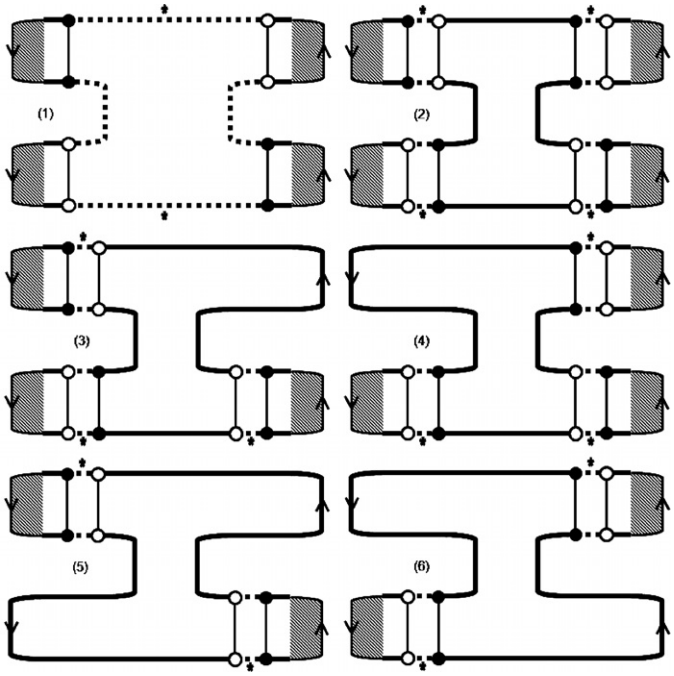

Figure 4. The six sets of topologically distinct diagrams that contribute to the dominant semiclassical term of the average shot-noise power.

Inserting the semiclassical values $W_1 \approx N^{-1}$, $W_2 \approx -N^{-3}$, (22), (23) and the defining expressions of the matrices C_1, C_2, T, R and L into (24), we obtain the compact result

$$\langle \mathbf{g}_2 \rangle = \frac{g_1^4 \bar{g}_2 + 2g_1^3 \bar{g}_1^2 + 2g_1^2 \bar{g}_1^3 + g_2 \bar{g}_1^4}{(g_1 + \bar{g}_1)^4} + \mathcal{O}(N^{-1}), \tag{25}$$

where $g_p = \sum_{i=1}^{N_1} (\Gamma_i)^p$ and $\bar{g}_p = \sum_{i=N_1+1}^{N} (\Gamma_i)^p$.

A similar calculation for $\langle \mathbf{g}_1 \rangle$ can be found in [20] which yields

$$\langle \mathbf{g}_1 \rangle = \frac{g_1 \bar{g}_1}{g_1 + \bar{g}_1} + \mathcal{O}(N^{-1}). \tag{26}$$

Inserting (25) and (26) into $\langle \mathbf{p} \rangle = \langle \mathbf{g}_1 \rangle - \langle \mathbf{g}_2 \rangle$ we obtain the dominant semiclassical value of the average shot-noise power

$$\langle \mathbf{p} \rangle = \frac{g_1^4 \bar{g}_1 + g_1^3 \bar{g}_1^2 - g_1^4 \bar{g}_2 - \bar{g}_1^4 g_2 + g_1^2 \bar{g}_1^3 + g_1 \bar{g}_1^4}{(g_1 + \bar{g}_1)^4} + \mathcal{O}(N^{-1}), \tag{27}$$

in agreement with Whitney's result obtained from the semiclassical trajectory approach [10]. Equation (27) reproduces the results of the cascade approach [24] if we set $g_p = N_1(\Gamma_1)^p$ and $\bar{g}_p = N_2(\Gamma_2)^p$, and is in agreement with semiclassical calculations via the generating function of full counting statistics [25, 26] if we set $N_1 = N_2 = N/2$, $g_p = N(\Gamma_1)^p/2$ and $\bar{g}_p = N(\Gamma_2)^p/2$.

3.2. Dominant quantum correction

When the matrix U in (20) is distributed according to the circular orthogonal ensemble, the average second moment $\langle \mathbf{g}_2 \rangle$, shown in equation (25), has a quantum correction of $\mathcal{O}(1)$

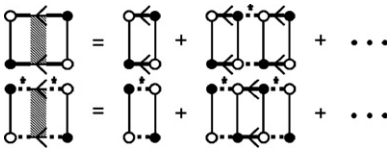

Figure 5. Diagrammatic representation of the functions f_{TT} (top), equation (32), and f_{UU} (bottom), equation (33). They are an infinite series of maximally crossed diagrams, known as cooperons [20].

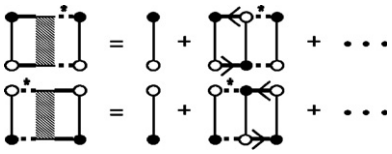

Figure 6. A series of maximally crossed diagrams representing the functions f_{TU} (top) and f_{UT} (bottom), equation (34), see [20].

which we denote as $\langle \delta \mathbf{g}_2 \rangle$. Physically, it emerges from constructive quantum interference between pairs of time-reversed electron paths. We separate this quantum correction into two contributions,

$$\langle \delta \mathbf{g}_2 \rangle = \langle \delta \mathbf{g}_{2,1} \rangle + \langle \delta \mathbf{g}_{2,2} \rangle. \tag{28}$$

The first term, $\langle \delta \mathbf{g}_{2,1} \rangle$, comes from the next order correction of the weights of the short U-cycles [20], $W_1 \approx N^{-1}(1 - N^{-1})$. This factor affects significantly the matrices F_L and F_R since after inserting $W_1^n \approx N^{-n} - nN^{-n-1}$ in equations (22) and (23) we obtain the corrections

$$\delta F_L = -\sum_{n=1}^{\infty} nN^{-n-1}\,\mathbf{Tr}(L^\dagger C_1 L)(\mathbf{Tr}(R^\dagger R))^{n-1} R^\dagger R = -\frac{\mathbf{Tr}(L^\dagger C_1 L)}{(N - \mathbf{Tr}(R^\dagger R))^2} R^\dagger R, \tag{29}$$

and

$$\delta F_R = -\sum_{n=1}^{\infty} nN^{-n-1}(\mathbf{Tr}(R^\dagger R))^{n-1}\mathbf{Tr}(T C_2 T^\dagger) R R^\dagger = -\frac{\mathbf{Tr}(T C_2 T^\dagger)}{(N - \mathbf{Tr}(R^\dagger R))^2} R R^\dagger. \tag{30}$$

Inserting $F_L + \delta F_L$ and $F_R + \delta F_R$ in the places of F_L and F_R of (24), with δF_L and δF_R given by (29) and (30), respectively, we obtain

$$\langle \delta \mathbf{g}_{2,1} \rangle = -2\frac{g_1^4 \bar{g}_2 + 2g_1^3 \bar{g}_1^2 - g_1^3 \bar{g}_1 \bar{g}_2 - g_1 g_2 \bar{g}_1^3 + 2g_1^2 \bar{g}_1^3 + g_2 \bar{g}_1^4}{(g_1 + \bar{g}_1)^5} + \mathcal{O}(N^{-1}). \tag{31}$$

The second correction to the second moment, $\langle \delta \mathbf{g}_{2,2} \rangle$, comes from diagrams of $\mathcal{O}(1)$. This correction has pure quantum characteristics and can be obtained via insertions of series of maximally crossed diagrams representing the discrete cooperon modes of the system. They can also be drawn as ladder diagrams [4], as shown in figures 5 and 6, and they are defined by the following equations:

$$f_{TT} = \sum_{n=0}^{\infty} N^{-n}(\mathbf{Tr}(R^\dagger R))^{n+1} = \frac{N\,\mathbf{Tr}(R^\dagger R)}{N - \mathbf{Tr}(R^\dagger R)}, \tag{32}$$

$$f_{UU} = \sum_{n=0}^{\infty} N^{-n-1}(\mathbf{Tr}(R^\dagger R))^{n} = \frac{1}{N - \mathbf{Tr}(R^\dagger R)} \tag{33}$$

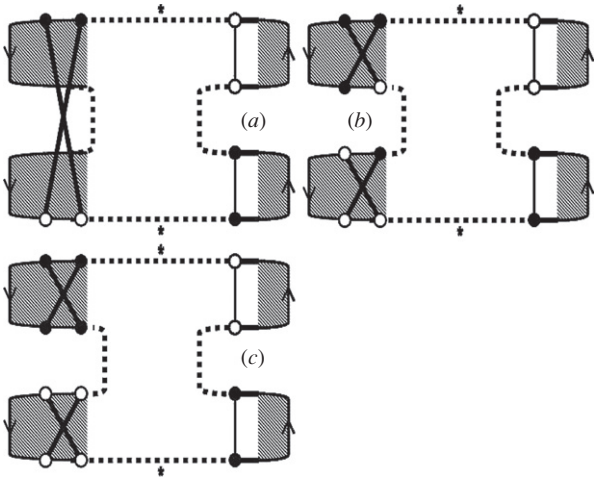

Figure 7. The first set of maximally crossed diagrams, which contribute to quantum correction of the shot-noise power. The diagrams are obtained by crossing the arms of the diagram of figure 4(1).

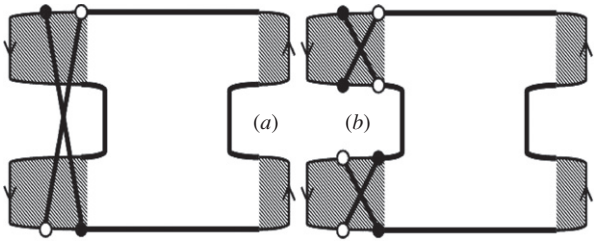

Figure 8. The second set of maximally crossed diagrams, which contribute to quantum correction of the shot-noise power. The diagrams are obtained by crossing the arms of the diagram of figure 4(2).

and

$$f_{TU} = f_{UT} = \sum_{n=0}^{\infty} N^{-n} (\mathbf{Tr}(R^{\dagger}R))^n = \frac{N}{N - \mathbf{Tr}(R^{\dagger}R)}. \tag{34}$$

We can systematically generate diagrams of $\mathcal{O}(1)$ by crossing the arms of the six diagrams of figure 4 inserting the diagrams of figures 5 and 6 in all topologically distinct ways. We found one set of diagrams with six elements, three sets with seven elements and two sets with three elements. They are shown in figures 7–9. The corresponding algebraic expressions are shown in table 2. The procedure is straightforward and is described in the following. We start by defining seven basic types of insertions, H_1, H_2, H_3, H_4, K_1, K_2 and K_3, whose diagrams and corresponding algebraic expressions are shown in the appendix. The diagrams of figure 7 are obtained by inserting K_1, K_2 and K_3 into the diagram of figure 4(1). The diagrams of figure 8 are obtained by inserting H_1 and H_2 into the diagram of figure 4(2). Finally, the diagrams of figure 9 are obtained by inserting H_3 and H_4 into the diagrams of figure 4(3)–(6).

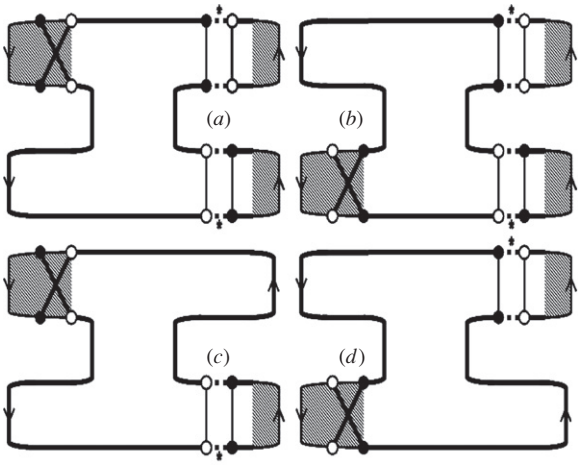

Figure 9. The third set of maximally crossed diagrams, which contribute to quantum correction of the shot-noise power. The diagrams are obtained by crossing the arms of the diagram of figure 4(3)–(6).

Table 2. Algebraic expressions for the diagrams of figures 7–9.

	1	2	3
a	$4W_2K_1\,\mathbf{Tr}(F_L)\mathbf{Tr}(F_R)$	$4\,\mathbf{Tr}(H_1H)$	$2W_1^2\,\mathbf{Tr}(H_3RR^\dagger)\mathbf{Tr}(F_L)\mathbf{Tr}(F_R)$
b	$2W_3K_2\,\mathbf{Tr}(F_L)\mathbf{Tr}(F_R)$	$2\,\mathbf{Tr}(H_2H)$	$2W_1^2\,\mathbf{Tr}(H_4R^\dagger R)\mathbf{Tr}(F_L)\mathbf{Tr}(F_R)$
c	$2W_2K_3\,\mathbf{Tr}(F_L)\mathbf{Tr}(F_R)$		$2W_1\,\mathbf{Tr}(H_3TC_2T^\dagger)\mathbf{Tr}(F_L)$
d			$2W_1\,\mathbf{Tr}(H_4L^\dagger C_1L)\mathbf{Tr}(F_R)$

With the three sets of algebraic expressions shown in table 2, we obtain the following expression for $\langle\delta\mathbf{g}_{2,2}\rangle$:

$$\begin{aligned}\langle\delta\mathbf{g}_{2,2}\rangle = {} & 4W_2K_1\,\mathbf{Tr}(F_L)\mathbf{Tr}(F_R) + 2W_3K_2\,\mathbf{Tr}(F_L)\mathbf{Tr}(F_R) + 2W_2K_3\,\mathbf{Tr}(F_L)\mathbf{Tr}(F_R)\\ & + 4\mathbf{Tr}(H_1H) + 2\mathbf{Tr}(H_2H) + 2W_1^2\,\mathbf{Tr}(H_3RR^\dagger)\mathbf{Tr}(F_L)\mathbf{Tr}(F_R)\\ & + 2W_1^2\,\mathbf{Tr}(H_4R^\dagger R)\mathbf{Tr}(F_L)\mathbf{Tr}(F_R) + 2W_1\,\mathbf{Tr}(H_3TC_2T^\dagger)\mathbf{Tr}(F_L)\\ & + 2W_1\,\mathbf{Tr}(H_4L^\dagger C_1L)\mathbf{Tr}(F_R). \end{aligned} \tag{35}$$

Inserting the algebraic expressions for H_1, H_2, H_3, H_4, K_1, K_2 and K_3 shown in the appendix, equations (32)–(34) and the asymptotic value for the weights $W_1 \approx N^{-1}$, $W_2 \approx -N^{-3}$ and $W_3 \approx 2N^{-5}$ in (35), we obtain

$$\begin{aligned}\langle\delta\mathbf{g}_{2,2}\rangle = {} & -2(g_1+\bar g_1)^{-6}\big(-g_1^2\bar g_1^3\bar g_2 + 4g_1^3\bar g_1^2\bar g_2 + 4g_1^2\bar g_1^3 g_2 + 3g_1^4\bar g_1\bar g_2 - g_1^3\bar g_1^2 g_2 - 2g_2\bar g_1^5\\ & + 2g_1^5\bar g_3 + 2\bar g_1^5 g_3 - 4g_1^4\bar g_2^2 + 2g_1\bar g_1^3 g_2\bar g_2 + 2g_1^3\bar g_1 g_2\bar g_2 - 4g_1^2\bar g_1^2 g_2\bar g_2 - 2g_1^5\bar g_2 - 4g_2^2\bar g_1^4\\ & + 3g_1\bar g_1^4 g_2 + 2\bar g_1^4 g_3 g_1 + 2g_1^4\bar g_3\bar g_1 - 2g_1^4\bar g_1^2 - 4g_1^3\bar g_1^3 - 2g_1^2\bar g_1^4\big) + \mathcal{O}(N^{-1}). \end{aligned} \tag{36}$$

Inserting (31) and (36) into (28) we obtain the dominant quantum correction to the average second moment

$$\begin{aligned}\langle\delta\mathbf{g}_2\rangle = {} & 2(g_1+\bar g_1)^{-6}\big(-2g_1^3\bar g_1 g_2\bar g_2 + 4g_1^2\bar g_1^2 g_2\bar g_2 - 2g_1\bar g_1^3\bar g_2 g_2 + g_2\bar g_1^5 - 2g_1^5\bar g_3\\ & - 2\bar g_1^5 g_3 + 4g_1^4\bar g_2^2 + g_1^5\bar g_2 + 4g_2^2\bar g_1^4 + g_1^2\bar g_1^3\bar g_2 - 3g_1^3\bar g_1^2\bar g_2 - 3g_1^2\bar g_1^3 g_2 - 3g_1^4\bar g_1\bar g_2\\ & + g_1^3\bar g_1^2 g_2 - 3g_1\bar g_1^4 g_2 - 2\bar g_1^4 g_3 g_1 - 2g_1^4\bar g_3\bar g_1\big) + \mathcal{O}(N^{-1}). \end{aligned} \tag{37}$$

Let us now combine (25) with (37) and insert the proper dependence on Dyson's symmetry index β, via the factor $\left(\frac{2}{\beta}-1\right)$, to obtain the first two terms in the semiclassical expansion of the average second moment

$$\begin{aligned}\langle \mathbf{g}_2\rangle = {} & (g_1+\bar{g}_1)^{-4}\left(g_1^4\bar{g}_2+2g_1^3\bar{g}_1^2+2g_1^2\bar{g}_1^3+g_2\bar{g}_1^4\right)+2\left(\frac{2}{\beta}-1\right)(g_1+\bar{g}_1)^{-6}\left(-2g_1^3\bar{g}_1g_2\bar{g}_2\right.\\ & +4g_1^2\bar{g}_1^2g_2\bar{g}_2-2g_1\bar{g}_1^3\bar{g}_2g_2+g_2\bar{g}_1^5-2g_1^5\bar{g}_3-2\bar{g}_1^5g_3+4g_1^4\bar{g}_2^2+g_1^5\bar{g}_2\\ & +4g_2^2\bar{g}_1^4+g_1^2\bar{g}_1^3\bar{g}_2-3g_1^3\bar{g}_1^2\bar{g}_2-3g_1^2\bar{g}_1^3g_2-3g_1^4\bar{g}_1\bar{g}_2\\ & \left.+g_1^3\bar{g}_1^2g_2-3g_1\bar{g}_1^4g_2-2\bar{g}_1^4g_3g_1-2g_1^4\bar{g}_3\bar{g}_1\right)+\mathcal{O}(N^{-1}).\end{aligned} \tag{38}$$

The extension to $\beta=4$ of equation (38) can be made by using the diagrammatic rules for ensemble averaging over the CSE, see [20]. Note that if we set $\Gamma_i=1$ in (38), it simplifies to (14), as expected.

The corresponding analysis for the average conductance was presented in [20] and yields

$$\langle \mathbf{g}_1\rangle = \frac{g_1\bar{g}_1}{g_1+\bar{g}_1}+\left(1-\frac{2}{\beta}\right)\frac{g_2\bar{g}_1^2+g_1^2\bar{g}_2}{(g_1+\bar{g}_1)^3}+\mathcal{O}(N^{-1}). \tag{39}$$

Substituting (38) and (39) into $\langle \mathbf{p}\rangle = \langle \mathbf{g}_1\rangle - \langle \mathbf{g}_2\rangle$, we obtain the semiclassical expansion for the average shot-noise power with the dominant quantum correction:

$$\begin{aligned}\langle \mathbf{p}\rangle = {} & (g_1+\bar{g}_1)^{-4}\left(g_1^4\bar{g}_1+g_1^3\bar{g}_1^2-g_1^4\bar{g}_2-\bar{g}_1^4g_2+g_1^2\bar{g}_1^3+g_1\bar{g}_1^4\right)+\left(\frac{2}{\beta}-1\right)(g_1+\bar{g}_1)^{-6}\\ & \times\left(-3g_2\bar{g}_1^5+4g_1^5\bar{g}_3+4\bar{g}_1^5g_3-8g_1^4\bar{g}_2^2-3g_1^5\bar{g}_2-8g_2^2\bar{g}_1^4+4g_1^3\bar{g}_1g_2\bar{g}_2\right.\\ & +4g_1\bar{g}_1^3\bar{g}_2g_2-8g_1^2\bar{g}_1^2g_2\bar{g}_2-3g_1^2\bar{g}_1^3\bar{g}_2+3g_1^3\bar{g}_1^2\bar{g}_2+3g_1^2\bar{g}_1^3g_2+3g_1^4\bar{g}_1\bar{g}_2\\ & \left.-3g_1^3\bar{g}_1^2g_2+3g_1\bar{g}_1^4g_2+4\bar{g}_1^4g_3g_1+4g_1^4\bar{g}_3\bar{g}_1\right)+\mathcal{O}(N^{-1}).\end{aligned} \tag{40}$$

Equation (40) is the main result of this paper and is valid for $\beta\in\{1,2,4\}$. We recover the ideal contact case, equation (15), by setting $\Gamma_i=1$. If we make $g_p=N_1\Gamma_1^p$ and $\bar{g}_p=N_2\Gamma_2^p$ in (40), it simplifies to

$$\begin{aligned}\langle \mathbf{p}\rangle = {} & \frac{G_1G_2\left(G_1G_2(G_1+G_2)+G_1^3(1-\Gamma_2)+G_2^3(1-\Gamma_1)\right)}{(G_1+G_2)^4}\\ & +\left(\frac{2}{\beta}-1\right)\frac{G_1G_2(G_1-G_2)(G_1\Gamma_2+G_2\Gamma_1)\left(3\left(G_2^2-G_1^2\right)+4\left(G_1^2\Gamma_2-G_2^2\Gamma_1\right)\right)}{(G_1+G_2)^6},\end{aligned} \tag{41}$$

where $G_i=N_i\Gamma_i$ with $i=1,2$. This equation was obtained in [17] using both quantum circuit theory [25, 27] and diagrammatic perturbation theory.

The dominant quantum correction to the average shot noise power, equation (41), describes a subtle suppression/amplification transition on the dominant semiclassical value of the shot-noise power even without changing the parameter β that identifies the distinct symmetry classes. This effect can be modulated by controlling the barriers' transparencies and the number of channels in the leads. In figure 10, we show the effect comparing all symmetry classes CUE, COE and CSE. In the left panel, we show the transition as a function of the parameter $a=G_2/G_1$, whilst in the right panel we vary the barriers' transparencies in the case of symmetric contacts. Note in the latter case that the transition always occurs at $\Gamma=3/4$, independent of the parameters a and β. Another noteworthy feature of $\langle\delta p\rangle$ is its linear suppression in the opaque limit. This limit was defined in [10] as $\Gamma_i\to 0$ with G_i fixed. A similar effect for the weak-localization correction to the conductance has a nice physical explanation in the semiclassical approach [10]. In spite of being a small effect, the behavior

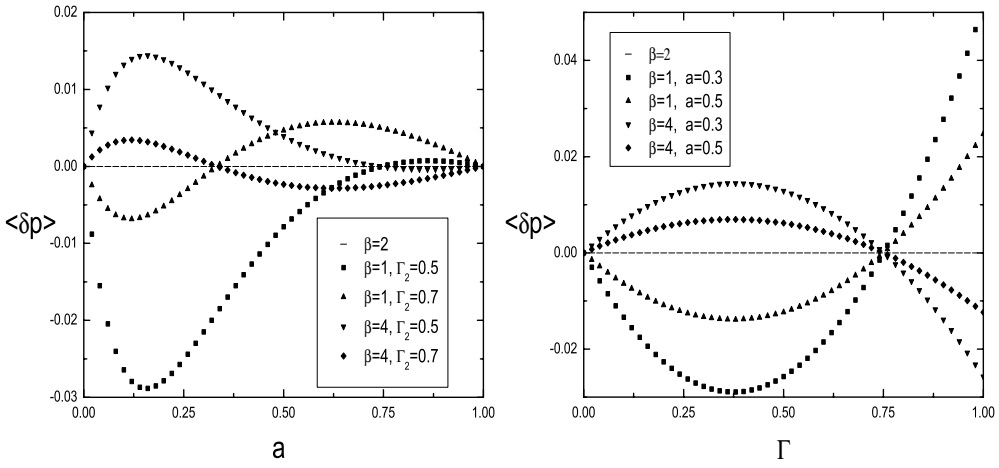

Figure 10. (Left) The dominant quantum correction to the average shot noise power, $\langle \delta p \rangle$, as a function of the parameter $a = G_2/G_1$ on the interval $0 \leqslant a \leqslant 1$ with fixed $\Gamma_1 = 0.3$. (Right) The dominant quantum correction as a function of the the barriers' transparencies in the symmetric case, where $\Gamma_1 = \Gamma_2 = \Gamma$. Note that all suppression–amplification transitions occur at $\Gamma = 3/4$.

of $\langle \delta p \rangle$ is unique in the sense that it is the largest observable effect that is a direct consequence of the combination of both temporal and spatial quantum coherences in the system.

4. Summary and conclusion

In this work, we presented a detailed quantitative analysis of the quantum correction to the average shot-noise power of a chaotic cavity with non-ideal contacts via the diagrammatic method for integration over the unitary group. Our main result is valid for all symmetry classes of the Wigner–Dyson's ensembles. We believe that this work provides a useful contribution to the development of the diagrammatic method by presenting a new set of maximally crossed diagrams that can be used for calculating the weak-localization correction of the average shot-noise power under more general conditions, such as those found in systems in the presence of symmetry breaking fields [15] or with ferromagnetic and/or superconducting reservoirs.

Acknowledgments

This work was partially supported by CNPq and FACEPE (Brazilian Agencies).

Appendix. Auxiliary diagrams

We present here the auxiliary diagrams, figures A1 and A2, and the corresponding algebraic expressions that are used to generate all maximally crossed diagrams:

$$H = W_1^2\,\mathbf{Tr}(F_L)\mathbf{Tr}(F_R)R^\dagger R R^\dagger + W_1\,\mathbf{Tr}(F_L)R^\dagger T C_2 T^\dagger + W_1\,\mathbf{Tr}(F_R)L^\dagger C_1 L R^\dagger \tag{A.1}$$

$$H_1 = \mathbf{Tr}\left(F_L F_R^T\right) f_{UU}^2 R + W_2 \mathbf{Tr}(F_L)\mathbf{Tr}(F_R) f_{TU}^2 R \tag{A.2}$$

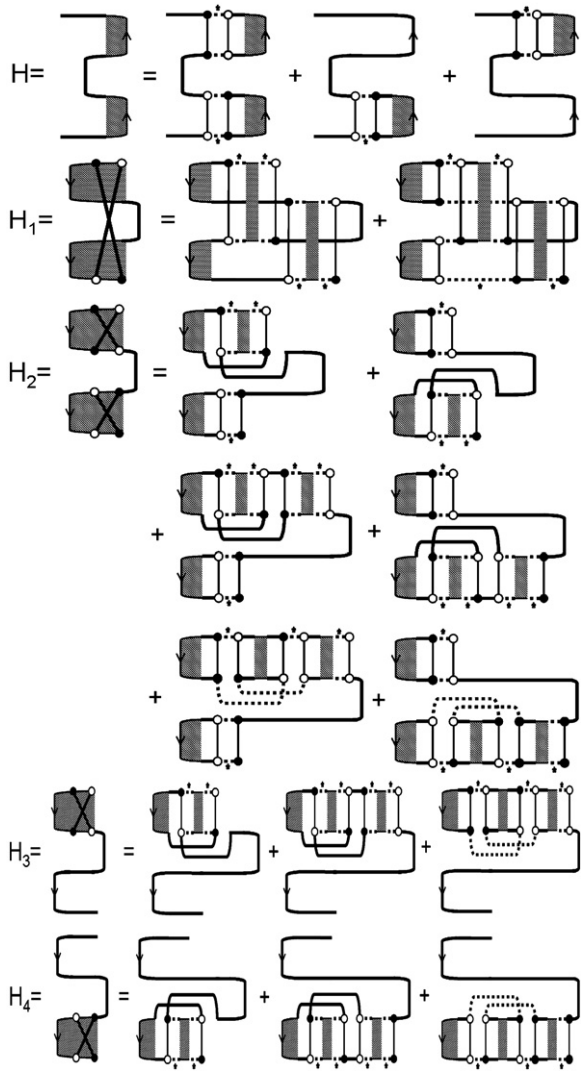

Figure A1. First set of auxiliary diagrams.

$$H_2 = W_1\,\mathbf{Tr}(F_R)\,f_{UU}\,F_L^T R + W_1\,\mathbf{Tr}(F_L)\,f_{UU}\,RF_R^T + W_1\,\mathbf{Tr}\left(RR^\dagger F_L^T\right) f_{UU}^2\,\mathbf{Tr}(F_R)R$$
$$+ W_1\,\mathbf{Tr}(F_L)\,f_{UU}^2\,\mathbf{Tr}\left(R^\dagger RF_R^T\right) R + W_1W_2\mathbf{Tr}(F_L)\,f_{TT}\,f_{TU}\mathbf{Tr}(F_R)R \quad (A.3)$$
$$+ W_1W_2\mathbf{Tr}(F_L)\,f_{TT}\,f_{TU}\mathbf{Tr}(F_R)R \quad (A.4)$$
$$H_3 = f_{UU}\,F_L^T\,TC_2T^\dagger + \mathbf{Tr}\left(RR^\dagger F_L^T\right) f_{UU}^2\,TC_2T^\dagger + W_2\mathbf{Tr}(F_L)\,f_{TT}\,f_{TU}\,TC_2T^\dagger \quad (A.5)$$
$$H_4 = L^\dagger C_1 LF_R^T f_{UU} + \mathbf{Tr}\left(R^\dagger RF_R^T\right) f_{UU}^2\,L^\dagger C_1 L + W_2\mathbf{Tr}(F_R)\,f_{TT}\,f_{TU}\,L^\dagger C_1 L \quad (A.6)$$
$$K_1 = W_2\,\mathbf{Tr}(F_L)\mathbf{Tr}(F_R)\,f_{TT}^2 + \mathbf{Tr}\left(F_LF_R^T\right) f_{UT}^2 \quad (A.7)$$
$$K_2 = \mathbf{Tr}(F_L)\mathbf{Tr}(F_R)\,f_{TT} + \mathbf{Tr}(F_L)\mathbf{Tr}(F_R)\,f_{TT} \quad (A.8)$$
$$K_3 = \mathbf{Tr}\left(RR^\dagger F_L^T\right)\mathbf{Tr}(F_R)\,f_{UU}\,f_{UT}\mathbf{Tr}(F_R) + \mathbf{Tr}\,(F_L)\,\mathbf{Tr}\left(R^\dagger RF_R^T\right) f_{UU}\,f_{UT}\mathbf{Tr}(F_R)$$
$$+W_2\mathbf{Tr}(F_L)\mathbf{Tr}(F_R)\,f_{TT}^2 + W_2\mathbf{Tr}(F_L)\mathbf{Tr}(F_R)\,f_{TT}^2.$$

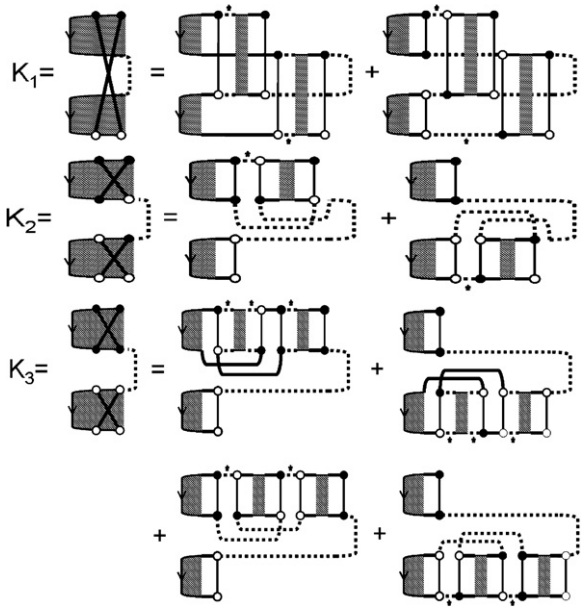

Figure A2. Second set of auxiliary diagrams.

References

[1] Datta S 2001 *Electronic Transport in Mesoscopic Systems* (Cambridge: Cambridge University Press)
[2] Beenakker C W J 1997 *Rev. Mod. Phys.* **69** 731
[3] Mello P A and Kumar N 2004 *Quantum Transport in Mesoscopic Systems: Complexity and Statistical Fluctuations* (Oxford: Oxford University Press)
[4] Akkermans E and Montambaux G 2007 *Mesoscopic Physics of Electrons and Photons* (Cambridge: Cambridge University Press)
[5] Nazarov Y V and Blanter Y 2009 *Quantum Transport: Introduction to Nanoscience* (Cambridge: Cambridge University Press)
[6] Blanter Ya M and Büttiker M 2000 *Phys. Rep.* **336** 1
[7] For a review, see Nazarov Y V (ed) 2002 *Quantum Noise in Mesoscopic Physics* (Dordrecht: Kluwer)
[8] Gustavsson S, Leturcq R, Simovic B, Schleser R, Ihn T, Studerus P, Ensslin K, Driscoll D C and Gossard A C 2006 *Phys. Rev. Lett.* **96** 076605
[9] Gustavsson S, Leturcq R, Ihn T, Ensslin K, Reinwald M and Wegscheider W 2007 *Phys. Rev.* B **75** 075314
[10] Whitney R S 2007 *Phys. Rev.* B **75** 235404
[11] Brouwer P W 2007 *Phys. Rev.* B **76** 165313
[12] Whitney R S, Jacquod P and Petitjean C 2008 *Phys. Rev.* B **77** 045315
[13] Braun P, Heusler S, Müller S and Haake F 2006 *J. Phys. A: Math. Gen.* **39** L159
[14] Savin D V and Sommers H-J 2006 *Phys. Rev.* B **73** 081307
[15] Béri B and Cserti J 2007 *Phys. Rev.* B **75** 041308
[16] Mehta M L 1991 *Random Matrices* (New York: Academic)
[17] Ramos J G G S, Barbosa A L R and Macêdo A M S 2008 *Phys. Rev.* B **78** 235305
[18] Dyson F J 1962 *J. Math. Phys.* **3** 140
Dyson F J 1962 *J. Math. Phys.* **3** 157
[19] Mello P A and Baranger H U 1999 *Waves Random Media* **9** 105
[20] Brouwer P W and Beenakker C W J 1996 *J. Math. Phys.* **37** 4904
[21] Texier C and Montambaux G 2004 *Phys. Rev. Lett.* **92** 186801

[22] Samuel S 1980 *J. Math. Phys.* **21** 4061
[23] Macedo Junior A F and Macêdo A M S 2006 *Nucl. Phys.* B **752** 439–75
[24] Nagaev K E, Samuelsson P and Pilgram S 2002 *Phys. Rev.* B **66** 195318
[25] Macêdo A M S and Souza A M C 2005 *Phys. Rev.* E **71** 066218
[26] Barbosa A L R and Macêdo A M S 2005 *Phys. Rev.* B **71** 235307
[27] Campagnano G and Nazarov Yu V 2006 *Phys. Rev.* B **74** 125307